35th Annual International Conference of the IEEE EMBS
Osaka, Japan, 3 - 7 July, 2013

Calculating the Induced Electromagnetic Fields in Real Human Head by Deep Transcranial Magnetic Stimulation *

Mai Lu[1] and Shoogo Ueno[2]

Abstract— **Stimulation of deeper brain structures by transcranial magnetic stimulation (TMS) may be beneficial in the treatment of several neurological and psychiatric disorders. This paper presents numerical simulation of deep transcranial magnetic stimulation (dTMS) by considering double cone, H- and Halo coils. Three-dimensional distributions of the induced fields i.e. magnetic flux density, current density and electric fields in realistic head model by dTMS coils were calculated by impedance method and the results were compared with that of figure-of-eight coil. It was found that double cone and H-coils have significantly deep field penetration at the expense of induced higher and wider spread electrical fields in superficial cortical regions. The Halo coil working with a circular coil carrying currents in opposite directions provides a flexible way to stimulate deep brain structures with much lower stimulation in superficial brain tissues.**

I. INTRODUCTION

Transcranial magnetic stimulation (TMS) is a technique that applies a brief magnetic pulse to the scalp and underlying cortex, changing the pattern of neuronal firing and producing a localized axonal depolarization [1][2][3]. TMS has promise as a non-invasive, non-pharmacological, and safe treatment. It has been used for anatomic brain mapping and for diagnostic and therapeutic purposes [4].

Although TMS treatment for depression with a common target in the dorsolateral prefrontal cortex has improved over the last years [5], current TMS methodologies do not yet yield the desired results, especially for major depressive disorder which is a highly prevalent and disabling condition associated with significant morbidity and mortality [6-7]. Many studies indicate that reward circuit is the focus in the study of depression [8-9]. There is a reason to assume that activation of deeper prefrontal and limbic regions may increase the antidepressant effect. The promising targets for dTMS can be the subgenual anterior cingulate cortex and the nucleus accumbens which lie at depths of approximately 60 and 70 mm, respectively, or the orbitofrontal, medial frontal cortices, and the frontal pole which lie at depths of 30 to 40 mm and have strong connectivity to anterior cingulate cortex [10-11].

To stimulate deeper neuronal regions such as reward-related pathways directly, much higher stimulation intensities are needed, as the electric field decreases rapidly as a function of tissue depth. However, even if stimulation intensities could be highly increased at the source, the use of standard TMS coils (such as round or figure-of-eight coils) at such high stimulation intensities does not allow safe stimulation and can lead to undesirable side effects. These limitations have led to the development of novel coil designs suitable for dTMS, which allows direct stimulation of much larger and deeper brain regions by significant reduction of the decay rate. In the past decade, there are several coil configurations potentially suitable for dTMS: double cone, H- and Halo coils [12][13][14].

II. COIL DESIGNS FOR DEEP TRANSCRANIAL MAGNETIC STIMULATION

Three coil types for dTMS have been numerically designed as shown in Fig. 1, where Fig. 1(a)-(c) show the double cone, H- and Halo coils which are placed on the surface of the head model. For comparison, Fig. 1(d) shows the modelled figure-of-eight coil.

The double cone coil was composed with two large circular coils with a fixed angle (95 deg) between them. The inner and outer radii of the circular wings are 70 mm and 20 mm, respectively. The number of the wire turns in each wing is 10. The H-coil with complicated winding was composed of a base portion and return portions. The coil is designed to minimize the unintended stimulation of portions of the brain, while reducing the accumulation of the surface charges. The Halo coil with 5 turns has inner and outer radii of 138 and 150 mm, respectively. It is operated simultaneously with a typical circular coil carrying currents in opposite directions (Halo-circular coil assembly). The circular coil with mean diameter 90 mm and 14 turns is located 100 mm above the Halo coil. For comparison, we have also modeled the figure-of-eight coil. The inner and outer radii of the circular wings are 10 mm and 50 mm, respectively. The number of the wire turns in each wing is 10. For purposes of comparison with the stimulation results obtained by figure-of-eight coil, a pulse current with amplitude of I=7.7 kA and working frequency 3.6 kHz in a typical clinical application of figure-of-eight coil was fed into the double-cone, H- and Halo-coils.

III. IMPEDANCE METHOD

The human head model is described using a uniform 3D Cartesian grid and is composed of small cubic voxels. The size of each voxel is 1mm $\times$ 1mm $\times$ 1mm. Assuming that, in each voxel, the electric conductivities are isotropic

*This work is supported in part by the National Nature Science Foundation of China under contract No. 51267010.

[1]M. Lu is with the Key Lab. of Opt-Electronic Technology and Intelligent Control of Ministry of Education, Lanzhou Jiaotong University, Lanzhou, 730070, P. R. China mai.lu@hotmail.com

[2]S. Ueno is with Department of Applied Quantum Physics, Graduate School of Engineering, Kyushu University, Fukuoka 812-8581, Japan ueno@athena.ap.kyushu-u.ac.jp

978-1-4577-0216-7/13/$26.00 ©2013 IEEE

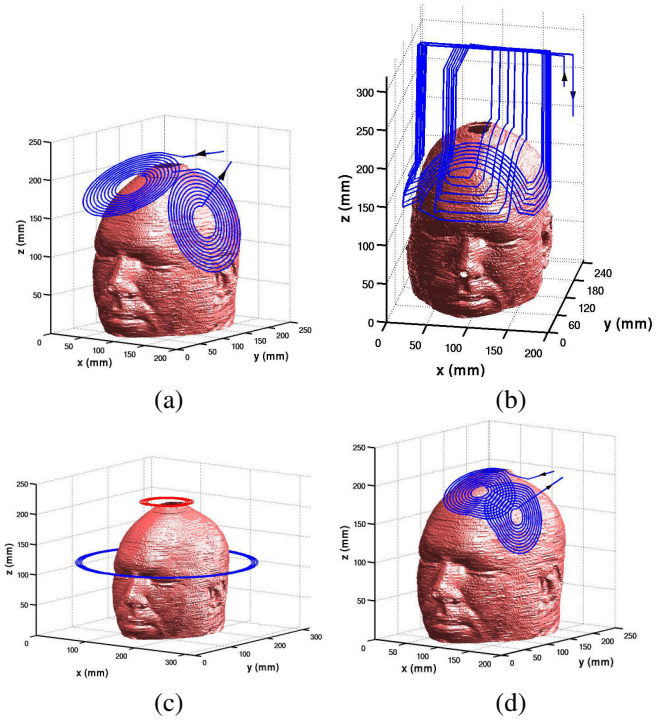

Fig. 1. Coil types for dTMS. (a) double cone coil, (b) H-coil, (c) Halo coil and (d) figure-of-eight coil.

and constant in all directions, the model is represented as a 3-D network of impedances. The magnetic flux density are calculated using Biot-Savart's law, the induced currents are calculated using the impedance method [15], and the induced electric fields are calculated using Ohm's Law. The impedance method has been found to be highly efficient as a numerical procedure for calculations of induced current densities and/or electric fields in tissue-classified anatomically based models [16][17][18].

TABLE I. TISSUE CONDUCTIVITIES AT f=3.6 kHz

Tissue	Conductivity $\sigma[S/m]$	Tissue	Conductivity $\sigma[S/m]$
Blood	7.00e-01	Lymph	5.27e-01
Blood vessel	3.11e-01	Mucous memb.	1.04e-03
Body fluid	1.50e-00	Cereb.spin.fluid	2.00e+00
Bone(cancellous)	8.21e-02	Nerve or spine	3.23e-02
Bone(cortical)	2.03e-02	Meninges	3.85e-01
Bone(marrow)	8.51e-02	Gray matter	1.07e-01
Cartilage	1.75e-01	White matter	6.56e-02
Fat	2.34e-02	Cerebellum	1.27e-01
Muscle	3.34e-01	Eye(cornea)	4.28e-01
Skin(dermis)	2.01e-04	Eye(lens)	3.33e-01
Tooth	2.03e-02	Eye(scle-wall)	5.08e-01
Glands	5.27e-01	Eye(aque.humo)	1.50e+00

IV. HUMAN HEAD MODEL AND TISSUE CONDUCTIVITY

In this study, we employed a 3D realistic human head model with 1 mm resolution as shown in Fig. 2. It was obtained from Brooks Air Force Laboratory (BAFL), USA. The head model which has 24 different tissues is based on anatomical slices from a male cadaver (1.8 m tall and 105 kg weight) originally from the Visible Human Project(VHP).

The electrical properties obtained from BAFL are modeled using the 4-Cole-Cole model [19]. In this model, the biological tissues subject to an electric field with angular frequency is modelled by relaxation theory and tissue properties can be obtained by fitting to experimental measurements [20]. The tissue conductivities used in the present calculations are shown in Table I.

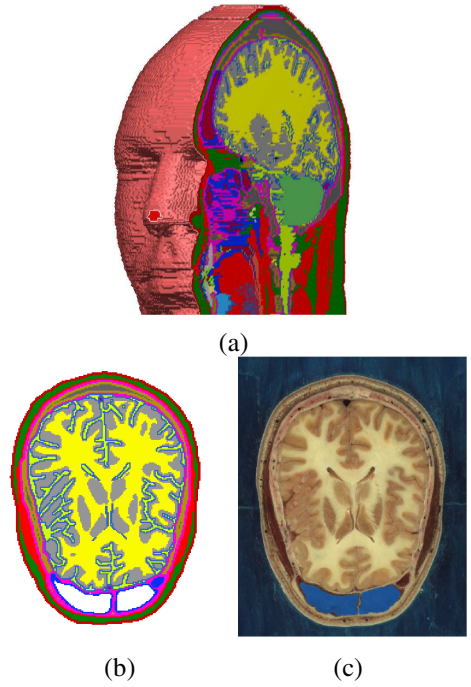

Fig. 2. Realistic head model. (a) Brooks model in 3D, (b) 2D Slice from Brooks model, (c) Anatomical slice image from VHP.

V. RESULTS AND DISCUSSIONS

Figs. 3(a)-(d) show the field intensity of magnetic flux density at the coronal plane of y=80 mm for double-cone, H-, Halo- and figure-of-eight coils, respectively. For each of the coils, the magnetic fields presents their maximum values at the coil surface and decay very quickly with increasing distance. It was also observed that double-cone and H-coils present slower rate of magnetic field decay than that of figure-of-eight coil. We should mention that the aspect ratio of Fig. 3(c) is different from the others because the dimension of Halo-coil is larger than that of double-cone, H- and figure-of-eight coils which makes the x-axis changes from 0 to 300 mm instead of 0-180 mm. In addition, the white color in these figures represents the magnetic fields with amplitude of zero.

Fig. 4(a)-(d) shows the field intensity of induced current density at the coronal plane of y=80 mm for double-cone, H-, Halo- and figure-of-eight coils, respectively. It was observed that double-cone and H-coils produce much higher current

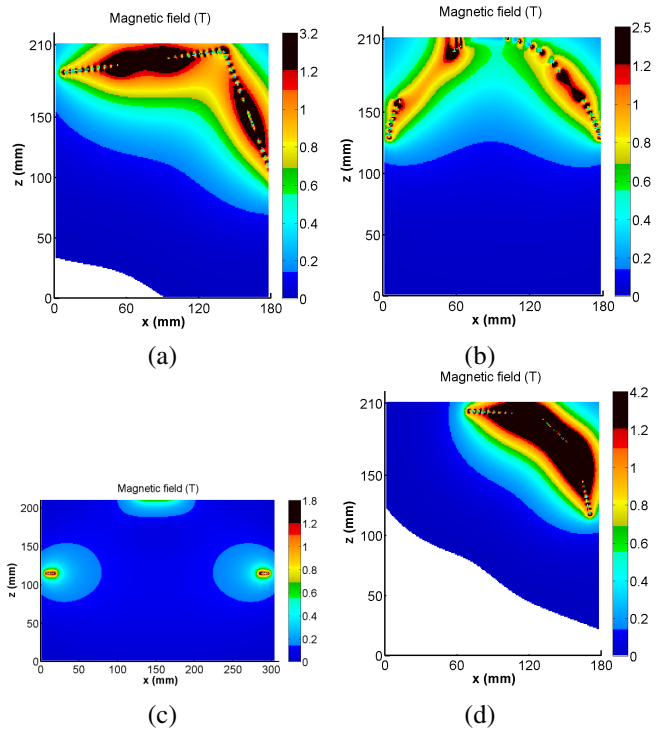

Fig. 3. Distributions of magnetic flux density on coronal slice of y=80 mm. (a) Double cone coil, (b) H-coil, (c) Halo-coil and (d) figure-of-eight coil.

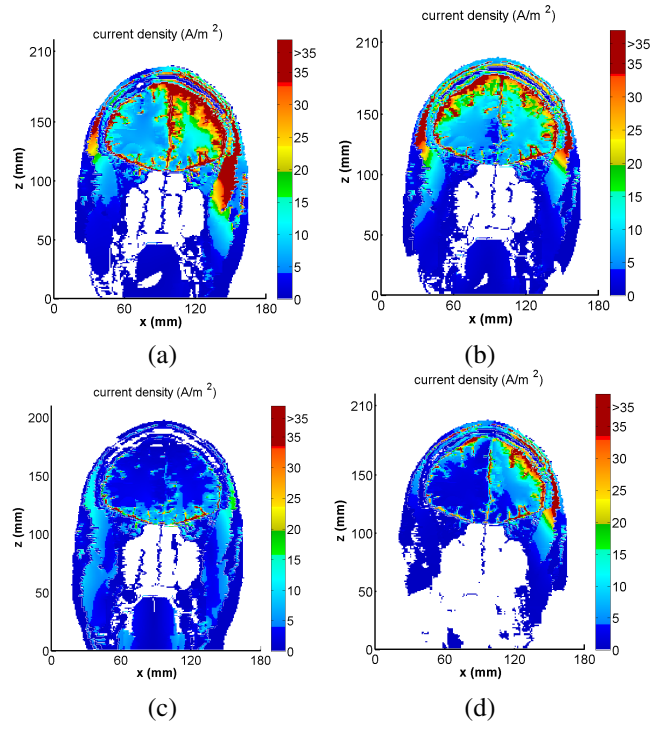

Fig. 4. Distributions of current density on coronal slice of y=80mm. (a) Double cone coil, (b) H-coil, (c) Halo-coil and (d) Figure-of-eight coil.

density in superficial cortical regions than that by figure-of-eight coil. On the contrary, the Halo coil presented higher current density in deep brain regions without inducing higher fields in cortical regions.

Fig. 5 shows the field intensity of electric fields along

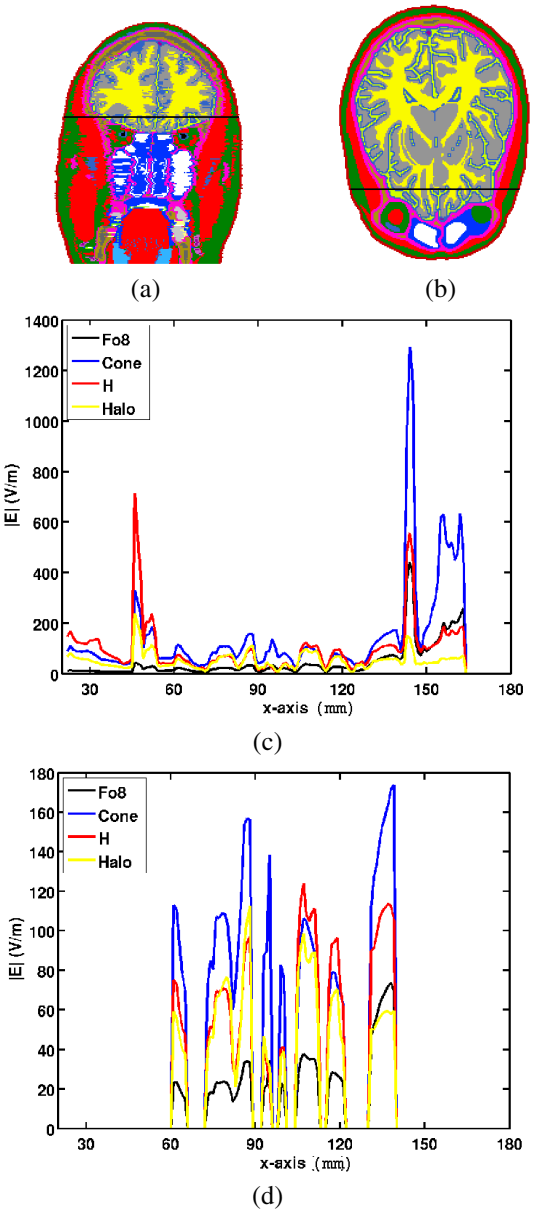

Fig. 5. Electric fields decay along the test line. (a) test line in the lateral-medial direction in coronal plane at y=80 mm, (b) test line in the lateral-medial direction in axial plane at z= 121 mm, (c) Electrical field intensity along the test line and (d) Electrical field intensity in brain tissues along the test line.

a test line in the lateral-medial direction for double cone, H-, Halo- and figure-of-eight coils. The test line is located in depth of 80 mm from the top of the head (Fig. 5(a)), and 80 mm from the front of the head (Fig. 5(b)). Fig. 5(c) demonstrated that the maximum induced electric field along the test line was presented in skull left side for all types of coils. Double-cone coil produces much strong electric fields (more than 600 V/m) in scalp and skull on the left side. H-

coil produces higher fields (more than 300 V/m) in skull on both left and right sides. If we only consider the induced electric fields in brain tissues (white matter, gray matter, cerebellum and spine) as shown in Fig. 5(d), we observed that the produced electric fields by Halo-coil is comparable with that by H-coil in the depth of 80 mm.

The distributions of the induced electric fields in the positions of 40 mm below the top of the head are shown in Figs. 6. In order to show the results more clearly, nonlinear colorbars are employed in these figures. The color palette is linear up to stimulation threshold 100 V/m and then constant (dark red) above threshold. It is observed that double cone and H- coils induce much higher electric fields with larger stimulation area in brain tissues in the depth of 40 mm than those by Halo- and figure-of-eight coils. From both Figs. 5 and 6, we know that the Halo coil working with a circular coil carrying currents in opposite directions provides a flexible way to stimulate deep brain structures with less induced fields in superficial cortical regions.

In this work, we have presented the induced electromagnetic fields in deep brain tissues by employing different deep TMS coils with fixed coil position and the same injected pulse currents. In the future, we intend to investigate the dependence of penetration depth on the coil positions and various pulse current protocols to realize focused induced fields in deep brain regions which are correlated to specific neural disorders. Eventually, we will create a mapping between deep transcranial magnetic stimulation coils and neural disorders to best be treated by them.

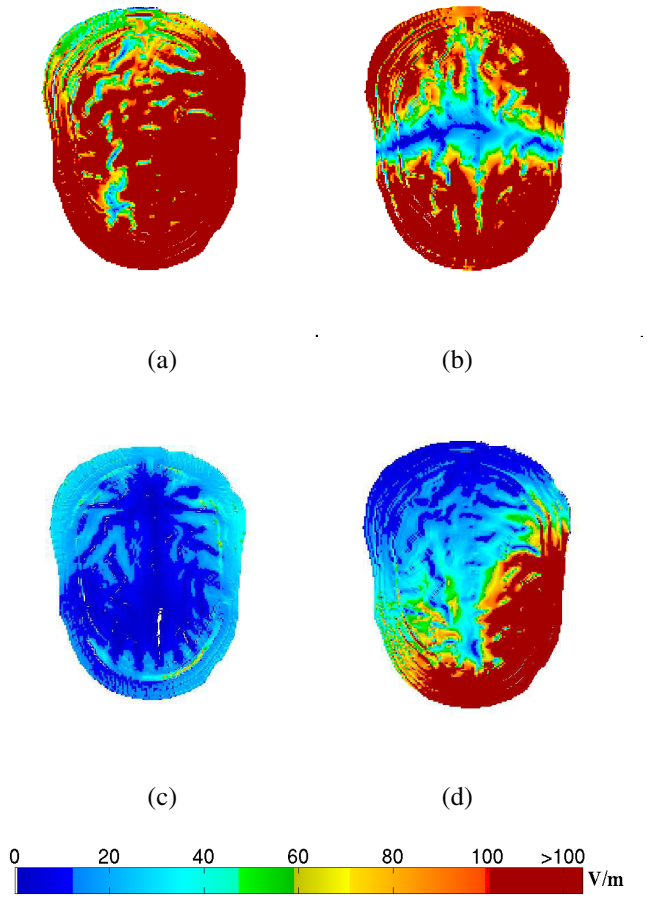

Fig. 6. Electric field distributions in an axial slice of 40 mm below the top of the head. (a) Double-cone coil, (b) H-coil, (c) Halo-coil and (d) figure-of-eight coil.

REFERENCES

[1] A.T. Barker, R. Jalinous and I.L. Freeston, Non-invasive magnetic stimulation of human motor cortex, Lancet, vol.1, pp. 1106-1107, 1985.

[2] S. Ueno, T. Tashiro, and K. Harada, Localized stimulation of neural tissues in the brain by means of a paired configuration of time-varying magnetic fields, J. Appl. Phys., vol. 64, no. 10, pp. 5862-5864, 1988.

[3] S. Ueno, T. Matsuda, and M. Fujiki, Functional mapping of the human motor cortex obtained by focal and vectorial magnetic stimulation of the brain, IEEE Trans. Magn., vol. 26, No. 5, pp. 1539-1544, 1990.

[4] T. Wagner, A. Valero-Cabre, and A. Pascual-Leone, Noninvasive human brain stimulation, Annu. Rev. Biomed. Eng., vol. 9, pp. 527-565, 2007.

[5] M. Gross, L. Nakamura, A. Pascual-Leone, and F. Fregni, Has repetitive transcranial magnetic stimulation (rTMS) treatment for depression improved? A systematic review and meta-analysis comparing the recent vs. the earlier rTMS studies. Acta Psychiatr Scand, vol. 116, pp. 165-173, 2007.

[6] H.K. Manji, W.C.Drevets, D.S. Charney, The cellular neurobiology of depression. Nat Med, vol. 7, pp. 541-547, 2011.

[7] C.B. Nemeroff, Recent advances in the neurobiology of depression, Psychopharmacol Bull, vol. 36, pp.6-23, 2002.

[8] H.C. Breiter and B.R. Rosen, Functional magnetic resonance imaging of brain reward circuitry in the human. Ann NY Acad Sci, vol. 877, pp. 523-547, 1999.

[9] P.W. Kalivas and N.D. Volkow, The neural basis of addiction: a pathology of motivation and choice. Am J Psychiatry, vol. 162, pp. 1403-1413, 2005.

[10] J.L. Price and W.C. Drevets, Neurocircuitry of mood disorders. Neuropsychopharmacology, vol. 35, pp. 192216, 2010.

[11] T.T. Yang, A.N. Simmons, S.C. Matthews, S.F. Tapert *et al.*, Depressed adolescents demonstrate greater subgenual anterior cingulate activity. Neuroreport, vol. 20, pp. 440-444, 2009.

[12] E.R. Lontis, M. Voigt, and J.J. Struijk, Focality assessment in transcranial magnetic stimulation with double and cone coils. J Clin Neurophysiol, vol. 23, pp. 462-471, 2006.

[13] Y. Roth, A. Zangen, and M. Hallett, A coil design for transcranial magnetic stimulation of deep brain regions. J Clin Neurophysiol, vol. 19, pp. 361-370, 2002.

[14] L.J. Crowthe, P. Marketos, P.I. Williams, Y. Melikhov, and D.C. Jiles, Transcranial magnetic stimulation: improved coil design for deep brain investigation. J. Appl. Phys., vol. 109, pp. 07B314, 2011.

[15] N. Orcutt and O.P. Gandhi, A 3-D impedance method to calculate power deposition in biological bodies subjected to time varying magnetic fields, IEEE Trans. Biomed. Eng., vol. 35, pp. 577-583, 1988.

[16] M. Lu and S. Ueno, Dosimetry of typical transcranial magnetic stimulation devices, J. Appl. Phys., Vol. 107, pp. 09B316, 2010.

[17] M. Lu and S. Ueno, Dosimetry of exposure of patients to pulsed gradient magnetic fields in MRI, IEEE Trans. Magn., vol. 47, pp. 3841-3844, 2011.

[18] M. Lu, S. Ueno, T. Thorlin, and M. Persson, Calculating the current density and electric field in human head by multichannel transcranial magnetic stimulation, IEEE Trans. Magn., vol. 45, pp. 1662-1665, 2009.

[19] K.S. Cole and R.H. Cole, Dispersion and absorption in dielectrics: alternating current characteristics, J. Chem. Phys., vol.9, pp. 341-351, 1941.

[20] S. Gabriel, R.W. Lau, and C. Gabriel, The dielectric properties of biological tissues: II. Measurements in the frequency range 10 Hz to 20 GHz, Phys. Med. Biol., vol. 41, pp. 2251-2269, 1996.